Title

Single cell and TCR analysis of immune cells from AAV gene therapy-dosed Duchenne muscular dystrophy patients.

Journal

Molecular Therapy: Methods & Clinical Development, 32(4)

ISSN

2329-0501

Authors

Emami, Michael
Brimble, Mark
Espinoza, Alejandro
et al.

Publication Date

2024-12-12

DOI

10.1016/j.omtm.2024.101349

Peer reviewed

Molecular Therapy
Methods & Clinical Development
Original Article

Single cell and TCR analysis of immune cells from AAV gene therapy-dosed Duchenne muscular dystrophy patients

Michael R. Emami,[1,10,11] Mark A. Brimble,[8,11] Alejandro Espinoza,[2] Jane Owens,[4] Laurence O. Whiteley,[5] Sandra Casinghino,[6] Thomas A. Lanz,[6] Philip K. Farahat,[7] Matteo Pellegrini,[3] Courtney S. Young,[10] Paul G. Thomas,[8] Elizabeth M. McNally,[9] S. Armando Villalta,[7] Stefan A. Schattgen,[8,12] and Melissa J. Spencer[1,12]

[1]Department of Neurology, David Geffen School of Medicine, University of California, Los Angeles, Los Angeles, CA 90095, USA; [2]Department of Human Genetics, University of California, Los Angeles, Los Angeles, CA 90095, USA; [3]Department of Molecular, Cell and Developmental Biology, and the Institute for Quantitative and Computational Biosciences – The Collaboratory, University of California, Los Angeles, Los Angeles, CA 90095, USA; [4]Pfizer Inc., Rare Disease Research Unit, Cambridge, MA 02139, USA; [5]Pfizer Inc., Drug Safety Research & Development, Cambridge, MA 02139, USA; [6]Pfizer Inc., Drug Safety Research & Development, Groton, CT 06340, USA; [7]Department of Physiology and Biophysics, University of California, Irvine, Irvine, CA 92697, USA; [8]Department of Host-Microbe Interactions, St Jude Children's Research Hospital, Memphis, TN 38105, USA; [9]Center for Genetic Medicine, Northwestern University Feinberg School of Medicine, Chicago, IL 60611, USA; [10]MyoGene Bio, San Diego, CA 92121, USA

Clinical trials for Duchenne muscular dystrophy (DMD) are assessing the therapeutic efficacy of systemically delivered adeno-associated virus (AAV) carrying a modified *DMD* transgene. High vector doses (>1E14 vg/kg) are needed to globally transduce skeletal muscles; however, such doses trigger immune-related adverse events. Mitigating these immune responses is crucial for widespread application of AAV-based therapies. We used single-cell RNA sequencing and T cell receptor (TCR) sequencing on peripheral blood mononuclear cells from five participants prior to, and after, dosing. One subject in the high-dose cohort experienced thrombotic microangiopathy (TMA). Few changes in cell frequencies occurred after treatment; however, differential gene expression demonstrated induction of interferon response genes in most T cell types. T cell clonotype and clumping analysis showed the expansion or appearance of groups of related TCR sequences in the post-treatment samples. Three of these expanded clumps could be assigned to prior human herpesvirus infections, two of which were present in the participant that exhibited TMA. These data provide insight on the mechanistic basis of human immune-AAV interactions and lay a foundation for improved understanding of why TMA arises in some patients and not others.

INTRODUCTION

Individuals with Duchenne muscular dystrophy (DMD) carry mutations in the *DMD* gene and experience progressive muscle degeneration and cardiomyopathy. *DMD* encodes for a 14-kDa mRNA, making the transgene impossible to fully package within a single adeno-associated virus (AAV) particle. Therefore, DMD transgenes intended for gene replacement therapy have been systematically modified into "micro- and mini-dystrophins" that carry the most important functional domains of dystrophin, and these vectors have demonstrated preclinical efficacy in small and large animal models.[1]

Innate and adaptive immune responses can arise to the capsid, cargo, or protein product of the transgene, leading to compromised safety and efficacy of AAV-based gene delivery. First-in-human trials showed that AAV delivery of a Factor IX transgene (under the control of a liver-specific promoter) produced elevation of liver enzymes and concomitant loss of circulating transgene product in some patients, attributed to T cell recognition of capsid peptides in hepatocytes.[2] When higher doses of AAV ($\geq$1E14 vg/kg) were used to target tissues like muscle and nerve, additional serious adverse events (SAE) arose, namely thrombotic microangiopathy (TMA) characterized by thrombocytopenia, acute kidney injury, and schistocytosis triggered by excessive activation of the complement pathway.[3] TMA has arisen shortly after AAV treatment for several diseases including DMD,[4,5] spinal muscular atrophy,[6] Fabry disease,[4,5] methylmalonic acidemia,[4,5] and Danon disease[4,5] and typically onsets within 3–6 days post-dosing. Investigations of clinical samples support involvement of the classical complement pathway in response to AAV dosing, which requires the presence of antibodies to the AAV capsid.[3]

Complement is a component of innate immunity that can be activated in three different manners: the classical pathway (mediated

Received 9 February 2024; accepted 27 September 2024;
https://doi.org/10.1016/j.omtm.2024.101349.

[11]These authors contributed equally

[12]Senior author

Correspondence: Melissa J. Spencer, Department of Neurology, David Geffen School of Medicine, University of California, Los Angeles, Los Angeles, CA 90095, USA.
E-mail: mspencer@mednet.ucla.edu

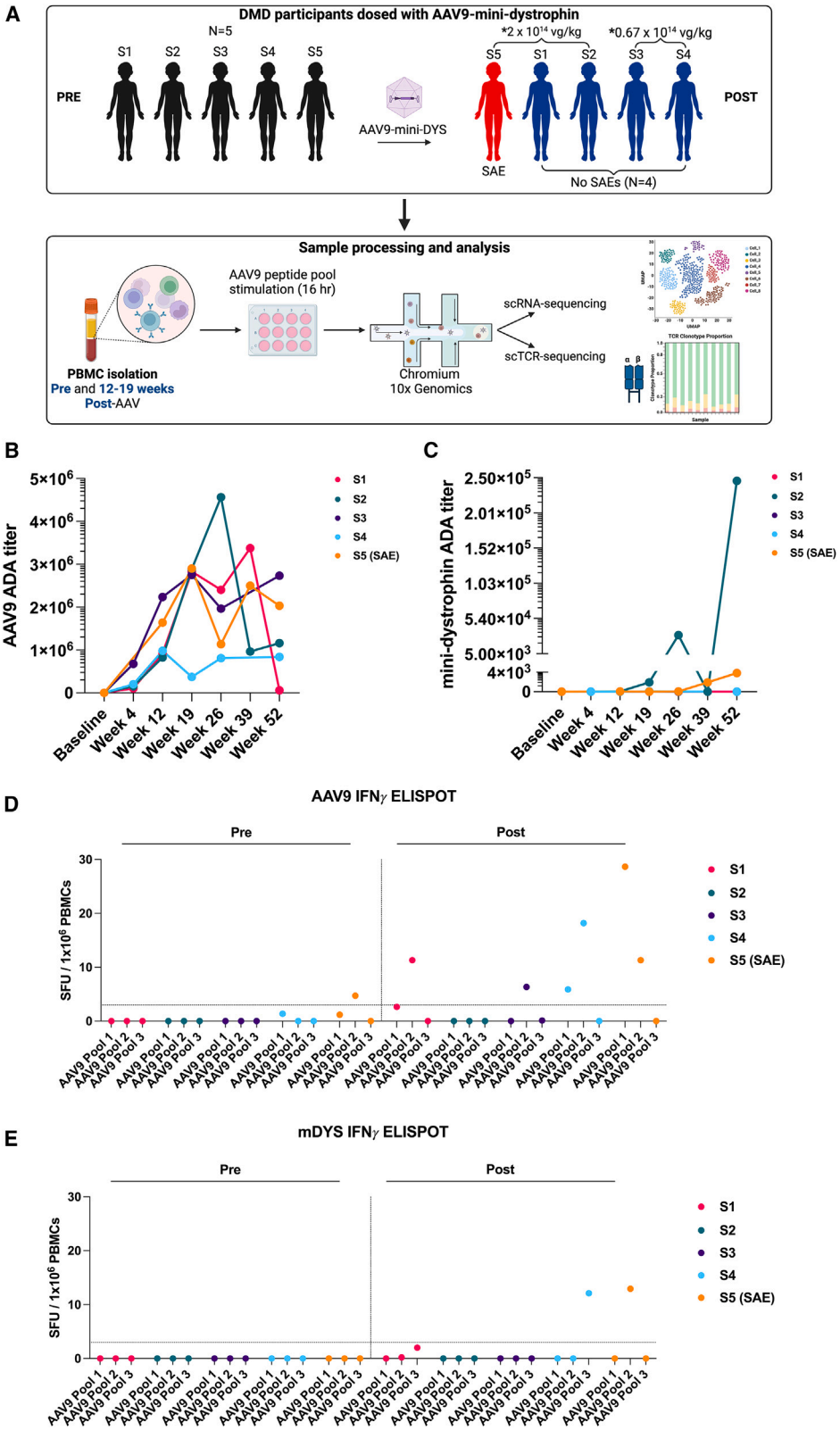

(legend on next page)

by C1q binding to anti-AAV on the capsid) the alternative pathway (which exists in homeostatic balance between activation and inhibition), and the lectin pathway. All three pathways generate C3 convertase that could exist as either [C3b + Bb] in complex or [C4b + C2a] in complex. In either case, C3 convertase cleaves C3, generating C3a and C3b split products, which in turn promote further immune reactions. *In vitro* studies demonstrated that human complement C3b can bind to AAV capsids and be converted to iC3b by Factor I[7] C5 convertase is formed when complement split products combine in different combinations, and cleave C5, leading to the appearance of C5a or C5b. Like C3a and C3b, these split products have a variety of pro-inflammatory and immune regulatory activities. For example, complement split products can promote humoral immunity by lowering the threshold for B cell activation,[8,9] and facilitate B cell class switching or somatic hypermutation in secondary lymphoid organs (SLOs).[10,11] Complement split products can also participate in T cell priming,[12] by promoting activation of antigen-presenting cells.[13,14] Eculizumab is a monoclonal antibody that recognizes complement C5, which has been used to reduce symptoms of TMA; however, eculizumab, is only partly to minimally effective in this setting. Thus, there is strong rationale for fully exploring how innate immune responses amplify downstream immunity to AAV.

Single-cell RNA sequencing analysis (scRNA-seq) provides a unique opportunity to obtain an unbiased and comprehensive profile of immune cell phenotypes and the relative frequencies of individual cell types. We conducted a within-subject analysis of peripheral blood mononuclear cells (PBMCs) and T cell receptor (TCR) clonal expansions from DMD patients who received AAV-mini-dystrophin in a phase 1b clinical trial. scRNA-seq of PBMCs revealed a dominant interferon response across most cell types, but few changes in cell frequencies. Paired-chain TCR clonotype analysis revealed an increased abundance of human herpesvirus (HHV)-specific CD8+ T cells in the post-dose samples of two donors, one of whom exhibited TMA. These findings will provide foundational knowledge about immune effectors involved in host-AAV-immune responses and demonstrates the utility of TCR sequencing in interrogating T cell responses after AAV delivery.

RESULTS

Clinical characteristics of DMD participants at baseline and after AAV9 mini-dystrophin gene therapy

This ongoing, non-randomized, open-label, ascending dose, phase 1b study (NCT03362502) was initiated in January 2018 at three sites in the United States. All subjects had a confirmed genetic diagnosis of DMD. See Figure 1 and Table 1 for information on subjects.

Following screening and baseline assessment (day −16), participants received a single intravenous infusion of low-dose or high-dose fordadistrogene movaparvovec (day 1). Subjects received either 0.67×10^{14} vg/kg (low-dose group) or 2.0×10^{14} vg/kg (high-dose group) AAV9 mini-dystrophin (PF-06939926, fordadistrogene movaparvovec).

Over the first 1 year of follow-up, visits occurred in the clinic (weeks 2, 4, 8, 12, 26, and 52) or remotely (weeks 3, 6, 10, 15, 19, 22, 32, and 39). Each participant was administered a pre-specified glucocorticoid regimen over the first 3 months of the study: a single intravenous dose of methylprednisolone (1–2 mg/kg) 1–4 h prior to receiving fordadistrogene movaparvovec infusion and daily oral prednisone or prednisolone post-treatment (1–2 mg/kg for the first 2–4 weeks, tapering to 1.0 mg/kg through the end of the first month, 0.75 mg/kg for the second month, and the higher of 0.50 mg/kg or the pre-study dose for the third month). After 3 months, participants resumed their baseline glucocorticoid regimen and remained on this regimen throughout the first year of follow-up except for adjustments due to side effects or changes in body weight. During the 6-week period of intensified immunosuppression, lymphocyte levels remained above 1,000/μL, apart from subject 3 with 870/μL lymphocytes on D14, and subject 5, with 870/μL lymphocytes at week 4. See Table 2 for select lab values for subjects at baseline and post-dosing.

One of the participants (subject 5) described in this article developed TMA, initially manifesting as severe acute kidney injury. On day 11 post-infusion, renal dysfunction was recognized by elevated creatinine levels to 7.5 mg/dL from a baseline of 0.2 mg/dL (normal range 0.3–0.7 mg/dL). The participant also had thrombocytopenia of 65×10^3/μL (normal range of 130–394 $\times 10^3$/μL), with evidence of hemodialysis by the presence of schistocytes, reduced haptoglobin, and of complement activation seen as reduced C3 levels. The participant was hospitalized and received intermittent hemodialysis treatment from day 15 to day 16. He also received intermittent renal dialysis treatments on days 17, 20, and 22. The participant received two doses (900 mg) of eculizumab, 1 week apart, with the first dose 15 days post-fordadistrogene movaparvovec infusion. The acute kidney injury markedly improved by 15 days after identification, at which point urine output was >800 mL per day. Both hematuria and proteinuria resolved after 38 days. The patient underwent genetic

Figure 1. DMD scRNA-seq and scTCR-seq experimental study design and subject characteristics

(A) Schematic outline of the study design. Five DMD patients were dosed with either 2E14 vg/kg or 0.67 vg/kg of AAV9 mini-dystrophin. (*) Doses initially provided as 3×10^{14} vg/kg and 1×10^{14} vg/kg, as calculated by ITR qPCR and adjusted here by correction factor using an updated transgene PCR titer method. Subject 5, dosed with 2E14 vg/kg experienced an adverse event of thrombotic microangiopathy. PBMCs were collected from the five DMD subjects at baseline and 12–19 weeks post-AAV administration. PBMCs were stimulated with AAV9 peptides for 16 h and then processed through 10x Genomics scRNA-seq and scTCR-seq. (B and C) Anti-AAV9 and anti-mini-dystrophin anti-drug antibodies (ADAs) measured at baseline and time points post-AAV administration. (D and E) IFNγ ELISpot responses against AAV9 and mini-dystrophin. Peptides spanning the coding sequence of AAV9 and mini-dystrophin were used to stimulate PBMCs. The horizontal line indicates the threshold cutoff.

Table 1. Subject characteristics and dosing

Subject	Age	Dose vg/kg	*DMD MUTATION*	% dystrophin baseline	% dystrophin 60 d post	NSAA baseline	NSAA day 90
1	6	2E14	Del *DMD* exons 49-52	0.2	86.1	28	31
2	7	2E14	Dup *DMD* c1259dupT	0.9	21.2	24	30
3	7	0.67E14	Point mut *DMD* exon 33 c4538del	4.1	9.8	24	26
4	9	0.67E14	Del *DMD* exons 46-47	0.2	12.5	30	29
5	12	2E14	Dup *DMD* exons 8-9	0.2	13	17	18

Age, mutations, dystrophin levels, and NSAA scores of the five Duchenne muscular dystrophy subjects dosed with AAV9-mini-dystrophin.

testing using the Genetic Renal Panel from the University of Iowa Molecular Otolaryngology and Renal Research Laboratories (Iowa City, IA, USA) and no pathogenic or likely pathogenic variants were reported.

Immune status at baseline and after AAV9-mini-dystrophin

Anti-drug antibody (ADA) titers against the AAV9 capsid and the mini-dystrophin transgene were measured before and after dosing (Figures 1B and 1C). Prior to dosing, none of the participants exhibited detectable anti-AAV9 titers. However, following administration of AAV9, a robust humoral response against the AAV9 capsid was observed in all five participants (Figure 1B). Only subject 2 developed anti-transgene antibodies, which became apparent at week 26, waned at week 39, and then greatly increased at week 52 (Figure 1C).

Evaluation of T cell responses to AAV9 and mini-dystrophin peptides were assessed by interferon (IFN)-γ enzyme-linked immunospot (ELISpot) at different time points before and after AAV9 administration (Figures 1D and 1E; Table S1). Four of five participants exhibited a positive IFN-γ ELISpot response to AAV9 capsid peptides for at least one specific time point post-AAV9 administration (Figure 1D), except for subject 2. Notably, participant 5, who experienced TMA, was the only subject to show a mildly positive IFN-γ ELISpot response to capsid at baseline, prior to AAV9 administration (Figure 1D). Two subjects showed a positive ELISpot response to mini-dystrophin peptides after dosing (subjects 4 and 5). While antibody and T cell responses were observed in a few of the subjects, none developed myositis, which has been observed in a small number of DMD patients after AAV-mini-dystrophin or micro-dystrophin treatment and has been attributed to a T cell-mediated transgene response.[15]

Single-cell RNA sequencing of PBMCs

PBMCs were collected from all five DMD subjects before ("pre") and 12–19 weeks after ("post") systemic delivery of AAV9 mini-dystrophin. PBMCs were evaluated by scRNA-seq to assess transcriptional changes on a single-cell basis and single-cell T cell receptor (TCR) V(D)J sequencing, which permits the identification of clonal T cells, indicative of prior activation and clonal expansion. Cryopreserved PBMCs were thawed and then stimulated for 16 h with a pool of 146 peptides spanning the AAV9 capsid, before single-cell capture and sequencing (Figure 1A; Table S2). Single-cell data (across participant samples and time points) were integrated using Seurat.[16] To assign cellular identities to the PBMCs, we utilized the Azimuth[17] program, which employs reference-based mapping, and subsequently identified 28 cell types (Figures 2A and 2B). No apparent cluster bias was observed among the five participants or between pre and post time points (Figure 2A).

Analysis of cell frequencies before and after AAV9-mini-dystrophin administration

Changes in cell type proportions were examined before and after AAV9-mini-dystrophin administration for all 28 cell subsets (Figures 2A, 2B, and S1). The proportions of 27/28 cell subsets remained relatively balanced between pre- and post-time points among nearly all cell types, suggesting that T cell frequencies were not greatly altered at the AAV9 treatment time point analyzed. Only the

Table 2. Laboratory values before and after dosing

	Platelets (#μL)			GGT (U/L)				Cardiac TNI (ng/mL)				
Subject	Day 1	Day 90	Day 135	Day 1	Day 7	Day 14	Day 45	Day 1	Day 7	Day 14	Day 30	Day 45
1	377,000	511,000	297,000	9	9	9	10	N/A	0.03	0.03	0.03	0.03
2	267,000	300,000	300,000	6	8	8	7	N/A	0.03	0.03	0.03	0.03
3	500,000	460,000	351,000	8	9	8	8	0.03	0.03	0.03	0.03	0.03
4	311,000	274,000	272,000	10	11	13	19	0.07	0.06	0.03	0.03	0.05
5	311,000	345,000	268,000	11	14	10	18	0.03	0.03	0.25	0.11	0.03

Clinical laboratory values for platelets, liver GGT, and cardiac TNI at the indicated time points.

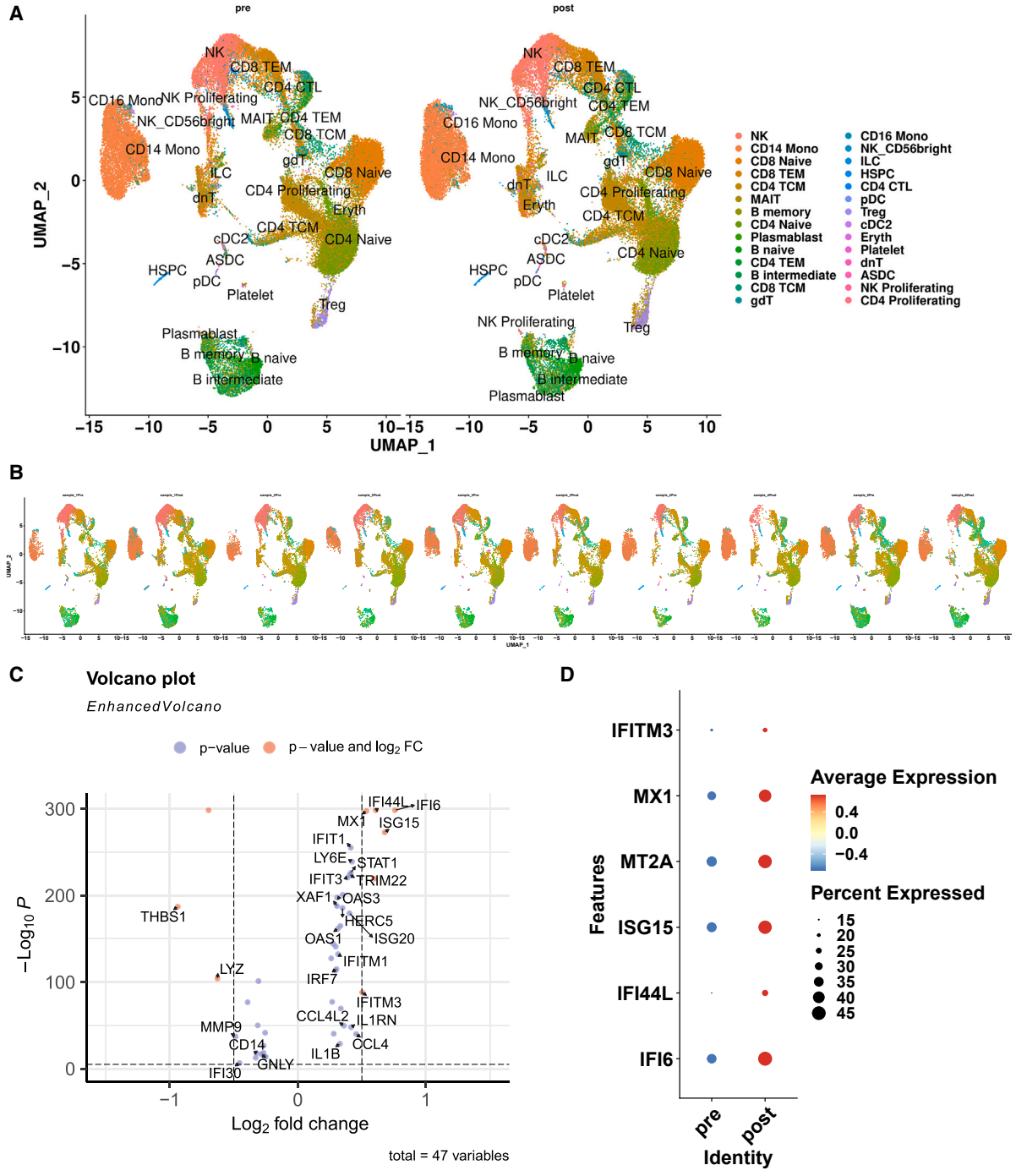

Figure 2. PBMC cell populations post- compared with pre-AAV-mini-dystrophin show a predominant interferon signature

(A) Azimuth annotation of cell types derived from five DMD subjects before (pre) and after (post)-AAV administration in a uniform manifold approximation and projection (UMAP) plot. Each dot represents a single cell and was colored according to cell type. (B) UMAP of PBMCs from each subject at each time point (pre- vs. post-dosing). (C) Volcano plot of differential gene expression in PBMCs post-PF06939926 compared with pre. Significantly up- and down-regulated genes contain Log_2(Fold Change) > 0.5 or Log_2(Fold Change) < 0.5 and -Log_{10}(*p* value) > 2.0. (D) Dot plot of significantly upregulated genes. Color is scaled by average expression and the dot size is proportional to the percentage of cells expressing the respective gene.

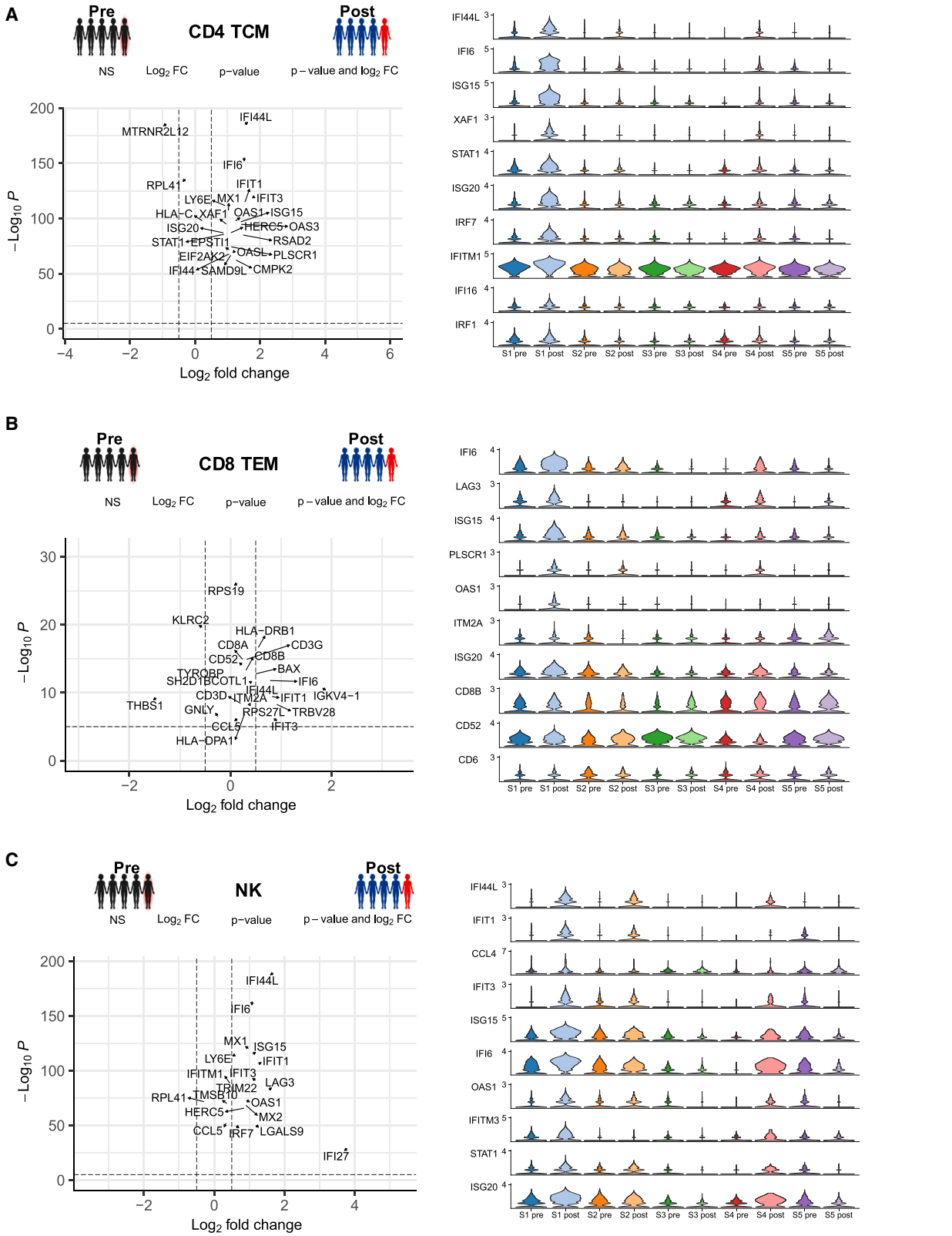

(legend on next page)

frequency of central memory CD4 T cells (CD4 T_{CM}) was statistically elevated post-AAV9 mini-dystrophin administration compared with pre-treatment (Figure S1).

Detection of an interferon response signature in numerous cell types after assessment of differentially expressed genes

Differential gene expression analysis was carried out on all PBMCs, comparing gene expression signatures pre- vs. post-dosing (Figure 2). This analysis revealed significant upregulation of genes known to be induced downstream of type I and II IFNs, including *IFI44L*, *IFI6*, *MX1*, *IFITM3*, and *MT2A* (Figures 2C and 2D, and Data S1). Gene set enrichment analysis (GSEA) was conducted, specifically probing gene ontology and biological processes (GO-BP), to explore the functional significance of the differentially expressed genes. Gene ontology terms associated with the defense response to virus and the response to type I interferon were observed to be the most significantly upregulated pathways (Figure S2). Downregulated genes were most highly associated with neutrophils and granulocytes.

Differential gene expression analysis was also carried out for each cell type, to compare gene signatures that arose after AAV9-mini-dystrophin. We focused first on CD4 T_{CM} cells because of the significantly elevated cell frequencies observed post-dosing (Figure 3A). This analysis revealed a similar upregulation of transcripts associated with type I and type II IFN responses, including *IFI44L*, *IFI6*, *ISG15*, *ISG20*, *MX1*, *IFIT1*, *IFIT3*, and *IRF7* (Figure 3A). However, when these genes were assessed in each condition in individual patients, the response appeared to be primarily driven by subject 1, with minimal induction of interferon response genes in subjects 2–5. Yet, when this same analysis was carried out for other cell types, the IFN response signature was not as skewed to subject 1 (Figures 3B, 3C, S3, and S4). Violin plots demonstrate that the induction of IFN response genes was most pronounced in subjects 1, 2, and 4. Notably, some interferon response genes were observed repeatedly across multiple cell types including *IFI6*, which showed significant upregulation in 16 cell types, while *ISG15* was upregulated in 10, *IFI44L* in nine, *IFITM1* in eight, *ISG20* in seven, and *IFITM3* and *STAT1* were upregulated in six cell types (Data S1).[18–22]

TCR clumping analysis categorizes T cells with known and unknown reactivities to AAV9-mini-dystrophin treatment

The diversity of viable TCR sequences an individual could generate is estimated to be up to approximately 1×10^{20}. However, it has been established that within a given human leukocyte antigen (HLA) context, TCRs responding to the same epitope have definable and similar receptor sequences and gene expression characteristics.[23–25]

To assess whether significantly similar TCR clonotypes were present within the overall dataset we used the TCR clumping algorithm within the CoNGA software tool. CoNGA generates two distance graphs: a uniform manifold approximation and projection (UMAP) of median gene expression for each TCR clonotype, and a TCR UMAP that plots the relational distances to all other TCR clonotypes within the dataset (Figure 4). Similarity matching against a literature database revealed the presence of several T cells with identifiable reactivity (Figure 5). Statistically enriched TCR clumps were then identified by quantifying similarities between TCR sequences both within the dataset and to a background dataset of shuffled sequences. Combined analysis of pre- and post-treatment timepoints identified several TCR clumps present within and across donors (Figure 5). As expected, TCR clumps mapped into gene expression space readily identified invariant iNKT and MAIT cell populations (Figure 5D). Further, several CD8+ T cell clumps were observed with elevated frequencies in the post-treatment samples of donors 1, 3, and 5 (Figures 5 and 6). Two of the CD8+ TCRs (clumps 4 and 5) were observed across multiple subjects (donors 1 and 3), and these were only seen in the post-treatment samples (Figures 5 and 6; Table S3). Clumps 4 and 5 each had four clonotypes that arose post-AAV dosing (Figure 6A) that were not detected in the pre-dose sample. Mapping of cells from these identified clumps onto the original gene expression UMAP showed colocalization primarily with the CD8 T_{EM} and T_{CM} populations (Figure 6B), and differential gene expression analysis showed a gene signature indicative of terminal effector CD8+ T cells (Figure 6C). Despite the limited number of T cells from the dataset for which epitope reactivity could be called with statistical confidence, database matching allowed identification of clumps 5, 6, and 7. All three clumps comprised TCRs reactive to known HHV epitopes (Table 3). Clump 5 was found to be reactive to a C07:02 CMV epitope from the UL29/28 protein (FRCPRRFCF) Clumps 6 and 7 were composed of TCRs reactive to known A02 restricted HHV reactive epitopes: a CMV pp65 (NLVPMVATV) and EBV BLMF1 (GLCTLVAML), respectively (Figure 6D). This participant experienced TMA, and the frequency of cells within both HHV reactive clumps was expanded in the post-AAV-treatment sample, with >0.65% of all T cells (approximately 1 in every 150 circulating T cells) assayed from the post-AAV-treatment sample of donor 5 belonged to these clumps.

The findings from this study, including the differential gene expression and TCR clonotype analysis, should be interpreted cautiously due to the limited sample size ($n = 5$). Despite this small sample size, these data highlight the potential of using TCR sequencing as a tool to partially decode the reactivities of peripheral T cells in patients receiving systemic treatment with AAV. Furthermore, the observations within the gene expression and

Figure 3. Differential gene expression profiling of PBMCs post-dose vs. baseline

(Left) Volcano plot of differential gene expression in individual cell types post-PF06939926 compared with pre-dose by cell type. (Right) Violin plots of selected differentially expressed genes, shown by patient and time point in individual cell types. Volcano plots of differential gene expression shown for CD4 TCM (A), CD8 TEM (B), and NK cells (C). Significantly up- and down-regulated genes contain Log_2(Fold Change) > 0.5 or Log_2(Fold Change) < 0.5 and -Log_{10}(*p* value) > 2.0. Volcano and violin plots for additional cell types are in Figures S3 and S4.

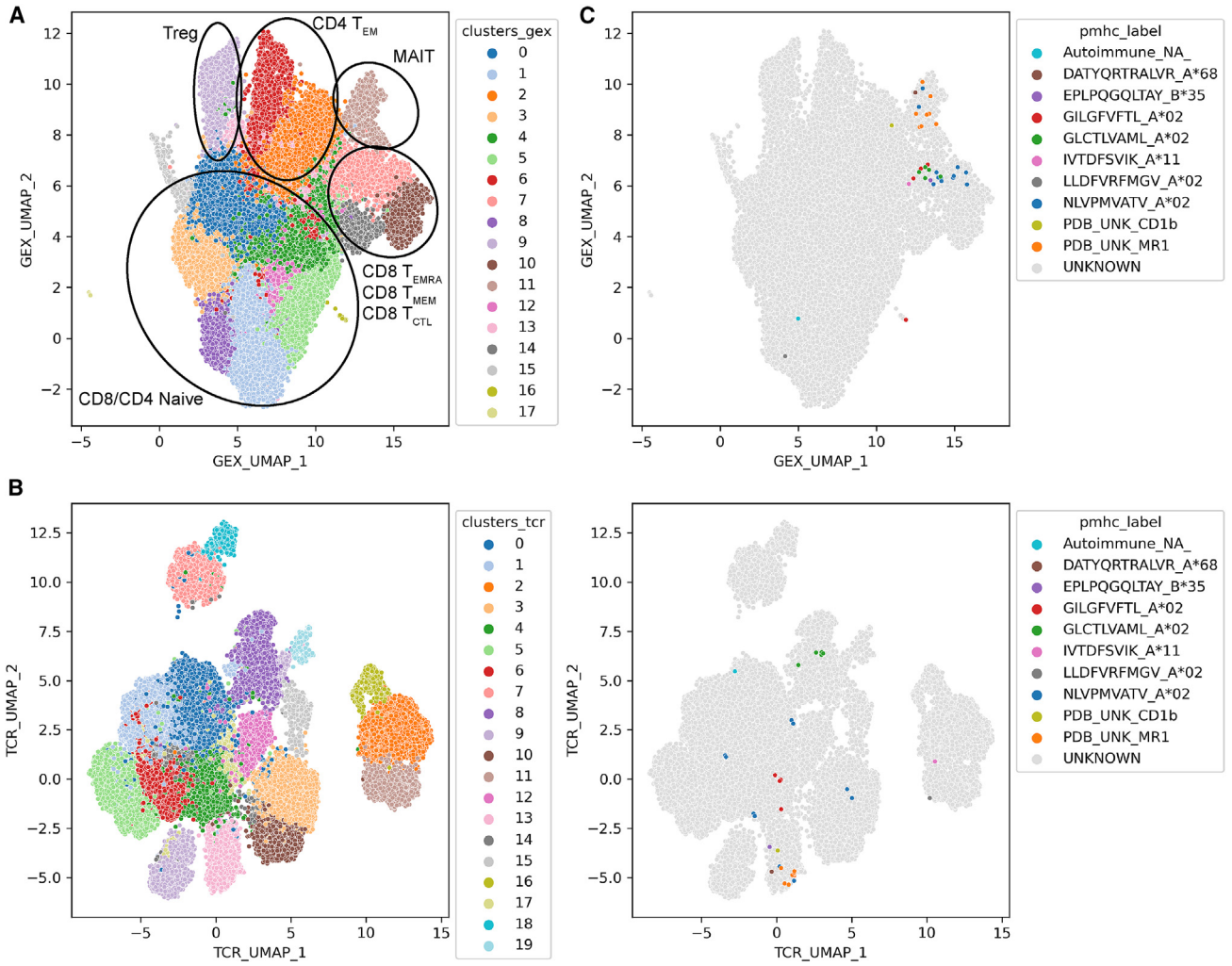

Figure 4. TCR clonotype similarity analysis of AAV9-mini-dystrophin treated patients

(A) ConGA Clonotype gene expression (left) and TCR clonotype (right) UMAP projection of T cells with paired-chain TCR information from all patients pre- and post-AAV9-mini-dystrophin. For GEX clusters, where a TCR clone abundance >1, the clonotype is reduced to, and plotted as, a single, median cell. (B) Plot of all T cell clonotypes with literature database identified reactivities overlayed on ConGA gene expression (left) and TCR (right) clonotype UMAPs. (C) Plot of all T-cell clonotypes with literature database identified reactivities overlayed on AonGA gene expression (left) and TCR (right) clonotype UMAPs.

TCR data provide a valuable reference for DMD patients receiving AAV gene therapy.

DISCUSSION

Innate and adaptive immune responses pose a significant challenge for safe and efficacious clinical application of AAV-based gene therapies. While initial results have shown promise for DMD clinical trials,[26] setbacks have been encountered including the need to pause trials to address complement activation-associated TMA.[27] High doses of immunosuppressive corticosteroids have been used surrounding the time of AAV dosing, which may also make patients susceptible to immune-related toxicities. TMA can be partly medically managed, but the downstream consequence of complement split product generation may still be problematic. Furthermore, capsid-specific antibodies and T cells may also lead to additional undesired immune responses to capsid or transgene, leading to liver toxicity and myositis, respectively. The need to define the range of immunological responses that arise in humans in response to AAV-based gene therapies is central to improving efficacy and safety.

Our analysis revealed that while cell frequencies did not significantly change post-AAV dosing, there was a shift in cellular phenotypes whereby multiple cell types were observed to upregulate transcripts related to type I and II interferons (IFNs). The pronounced upregulation of interferon response genes suggests a robust and coordinated immune response across various cell types, activating the interferon signaling pathway, which is crucial for the

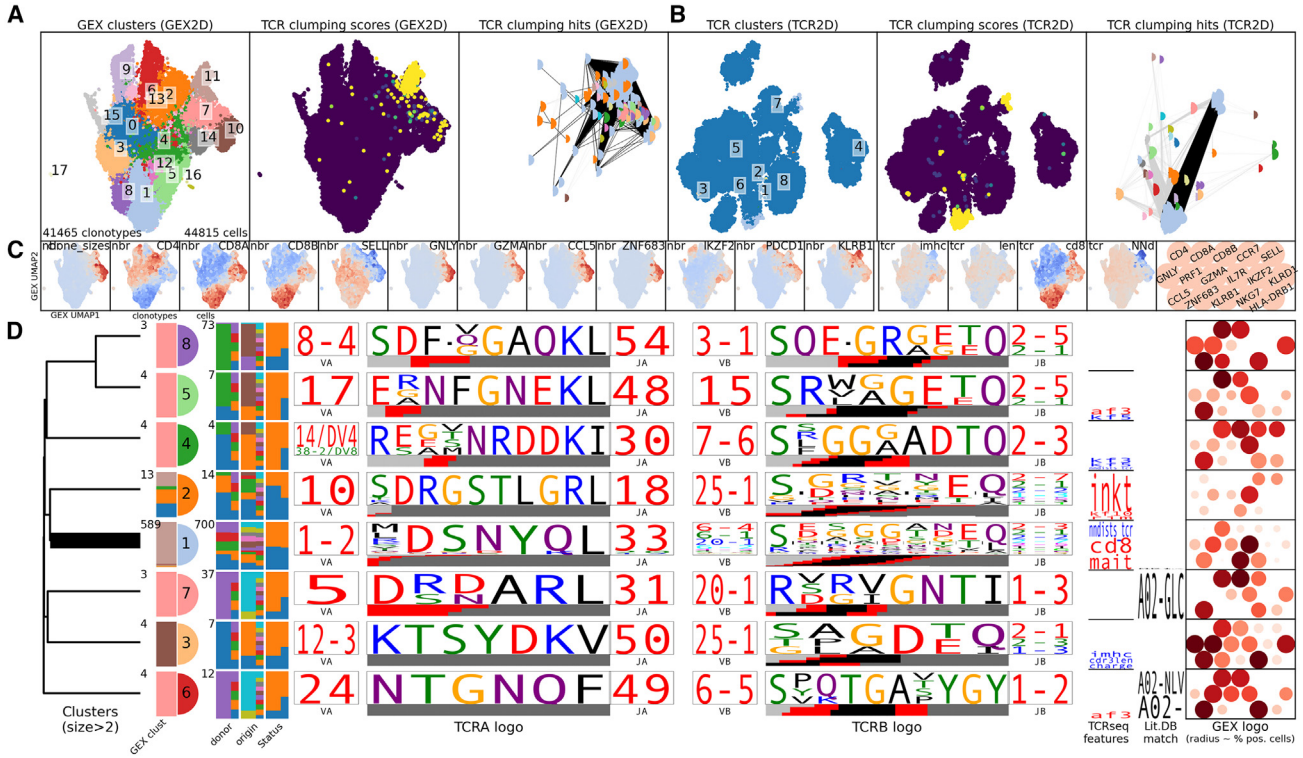

Figure 5. ConGA plot showing TCR clumping analysis with integrated gene expression

(A) ConGA map showing the gene expression clusters, TCR clumping scores, and TCR clumping hits in gene expression space (A) and TCR space (B). Positioning of identified statistically similar clonotypes and relative locations in gene expression and TCR space. (C) Expression heat maps for select T cell-related genes. (D) TCR clumping group results. Clumping group results are annotated (from left to right) 'Clonotypes' = the number of different TCR sequences within a clumping group; GEX cluster = vertical colored bar denoting the proportion of cells from a clumping group within a gene expression cluster in (A); colored semi-circle = the numerical identity of the TCR clumping group in (B); cells = the total number of T cells within the clumping group; Colored vertical bars show the proportion of cells originating from each; donor, origin (sample), and status (pre vs. post-AAV); amino acid sequence logo plots for (left) alpha and (right) beta chains of the TCR, showing V gene contribution, CDR3 amino acid sequence, and J gene contribution; TCRseqfeatures = sequences associated with a T cell phenotype (red = positively associated, blue = negatively associated); Lit.DB match = statistical similarity matching of sequences to previously identified epitope reactive TCRs; GEX logo = relative expression of select T cell-associated genes, and proportion of expressing cells within the TCR clumping group.

immune system's defense against viral infections.[28–33] This coordinated response may be facilitated through multiple mechanisms. For instance, antigen-presenting cells may activate T cells via viral peptide presentation, leading to the release of type I and II interferons.[34] These interferons can act in an autocrine fashion to induce the expression of interferon response genes in the T cell compartment.[35–37] Moreover, peptide stimulation could amplify immune responses in a paracrine fashion. Antigen-reactive CD4 and/or CD8 T cells secreting type I and II interferons and cytokines could activate other cell types such as monocytes and NK cells to induce the expression of interferon response genes, chemokines or cytokines.[36–38] While less is known about the immunological landscape following AAV administration, our findings align with studies investigating immune responses after adenoviral vaccination, SARS-CoV-2 (COVID-19) and Influenza infection.[39–45] These studies have demonstrated induction of interferon-stimulated and response genes, further supporting the relevance of our results.

The TCR sequence encodes the antigen-specificity information for an individual T cell. Despite the vast potential diversity of possible sequences, recent advances in quantifying TCR similarity have assisted in allowing identification of epitope restriction of T cells from sequence information alone.[24] While the landscape of validated TCR-epitope-pMHC combinations is highly restricted, we were able to use the sequence information from this dataset to identify the HHV-restricted reactivity of two large clonotype TCR clumps that were only elevated in the post-treatment sample of donor 5 (SAE) and a smaller population of CMV-specific cells found only in the post-treatment sample of donor 3. The expansion of HHV-related T cells in these individuals could represent evidence of latent herpes virus reactivation, a phenomenon that has been observed in the setting of TMA occurring after hematopoietic stem cell transplantation.[46,47] Renal transplant-associated TMA has also been observed in concordance with CMV infection.[48] Therefore, individuals with dormant or active CMV or EBV infections who receive AAV could be predisposed to TMA, especially in the setting of high-dose steroids

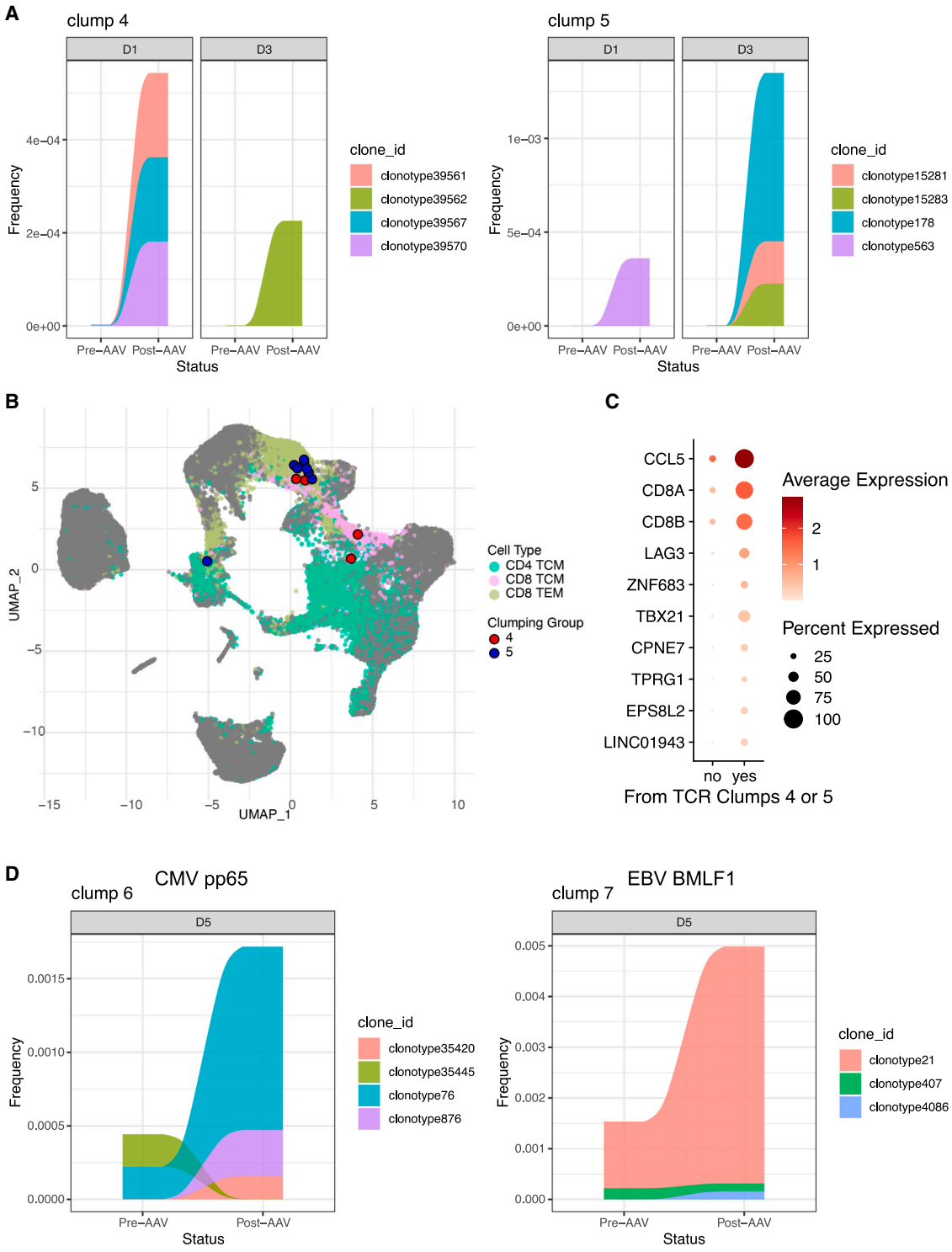

Figure 6. Expanded TCR clumps from subject 5 are associated with human herpes viruses

(A) Relative frequency of TCR clumps 4 (left) and 5 (right) within donors 1 and 3 pre- and post-AAV treatment. (B) Location of cells from clump 4 (red) and clump 5 (blue) overlayed on the full PBMC gene expression UMAP. (C) Dot plot of gene expression profiles of clumping groups 4 and 5 combined as compared with all other T cells in dataset. (D) Relative frequency of HHV reactive TCR clumps 6 (left) and 7 (right) within donor 5 pre- and post-AAV treatment.

Table 3. Non-invariant TCR clumps with identifiable reactivity

Clump	Virus:Protein	Epitope	HLA restriction	Donor	VDJdb matching
5	CMV:UL29/28	FRCPRRFCF	C07:02	3	Beta chain match
6	CMV:pp65	NLVPMVATV	A02:01	5	Paired chain match
7	EBV:BLMF1	GLCTLVAML	A02:01	5	Paired chain match

or other immunosuppressive regimens. This hypothesis needs extensive testing to be validated, but if true, could explain why some individuals develop TMA while others do not. It is possible that other clumps exhibiting similar expansion kinetics (i.e., clumps 4, 8, and 9) have similar viral protein specificities; however, their reactivity was not definable. Indeed, it is possible that these *undefinable* clumps are directly related to the AAV-infusion; however, validating their specificity against treatment-related epitopes would be required before they can be deemed treatment-associated.

Interestingly, despite the incubation with AAV9 peptides, there were no identifiable post-treatment clonotypes that appeared to express significantly elevated levels of TCR-activation induced genes. This observation may be explained by the fact that all patients were on steroids before and after their AAV doses, as it is usual to treat DMD patients with chronic glucocorticoids. It is also possible that the depth of scRNA-seq was insufficient for this task. The ELISPOT results from 400,000 PBMCs showed detectable but low levels of post-treatment AAV capsid and mini-dystrophin reactivity in some participants, whereas current 10x genomics per-reaction capacity stands at approximately 10,000 cells. Another interesting finding is that subject 5 who experienced TMA did not have an elevated interferon response signature as was seen in other participants. Future work should be conducted to ascertain if this is a recurrent phenomenon in individuals experiencing post-AAV TMA.

A caveat of this study is that the sample collections are restricted to a single pre- and post-infusion time point for each subject. The peripheral TCR repertoire is incredibly stable over time and although changes in clonal abundance after vaccination or infection can be readily identified, there may be only a short window of time in which such clones will be expanded, and thus visible within a peripheral sample examined at the single-cell resolution. Future studies using these technologies should consider the collection of multiple post-infusion timepoints where possible.

Our investigation benefits from a recent meta-analysis of over 250 AAV clinical trials, which aimed to identify risk factors influencing AAV immunity and efficacy.[4,5] The meta-analysis revealed considerable variability in the use of prophylactic or reactive immunosuppressants, which complicates interpretation. Additionally, assays used to determine anti-AAV neutralizing or binding antibody titers showed a wide range of methodologies and eligibility thresholds. Treatment-emergent serious adverse events (TESAEs) following AAV administration were also variable and may depend on a variety of factors, including AAV serotype, dosage, route of administration, and the disease indication and the recipients' immunological history. TMA was one of the most prominent TESAEs that was observed in the meta-analysis.

Recently, a study of 38 subjects dosed with AAV revealed that AAV-induced complement activation and TMA are dependent on the presence of anti-AAV capsid antibodies.[3] In our study, TMA was observed in one participant, subject 5; however, pre-dose screening did not reveal the presence of positive anti-AAV9 titers in this subject at baseline (Figure 1). On the other hand, subject 5 showed a rapid rise of anti-AAV9 antibodies 13 days post-dosing, concomitant with the TESAE (Table 1) suggesting that this subject may have indeed had prior AAV exposure. Support for this notion comes from the fact that subject 5 also showed a positive IFN-γ ELISPOT response to AAV9 at baseline, indicating the possibility of a pre-existing T cell memory response against the AAV9 capsid.

SAEs related to the mini/micro-dystrophin transgene have arisen in three of four DMD clinical programs including those sponsored by Pfizer, Sarepta-Roche, and Genethon.[15] Notably, all clinical trials for DMD deliver a mini-dystrophin transgene that contains exons 8–11, and the five participants who exhibited myositis all had genomic mutations that excluded those exons, indicating their first exposure to this region was from micro-dystrophin. This observation suggests a lack of tolerization to those regions of the protein, but this idea will need further experimental support. In our study, we did not have genomic mutations residing in this region (Table 1) and did not observe myositis, although subjects 4 and 5 exhibited a positive IFN-γ ELISPOT against the mini-dystrophin transgene post-dosing (Figure 1E). Subject 2 did not develop a positive ELISPOT despite having antibodies against mini-dystrophin at weeks 26 and 39 (Figure 1C). These anti-dystrophin responses do not appear to be consequential, since clinical myositis did not occur in any of these participants after exposure to the mini-dystrophin transgene. Prior studies demonstrated that some DMD patients harbor circulating T cells against dystrophin, in the absence of AAV dosing, and these T cells were decreased with steroid treatment.[49] The effect of these T cells on disease progression or whether their presence after AAV dosing predisposes to a myositis is not established.

Study limitations

Our study was limited by the small sample size and the specific comparisons involving small numbers of cells. This sample size underscores the need for further investigations with more AAV recipients to validate and reinforce the observed trends. Additionally, the presence of adverse events in some participants further emphasizes the

complexity of human immune responses to AAV and the need for careful interpretation of the results. In conclusion, our study provides preliminary evidence of immune activation, and changes to the peripheral TCR repertoire following AAV9 mini-dystrophin gene therapy in DMD patients. However, further investigations into immune responses in DMD patients post-AAV treatment are warranted to make firm conclusions regarding the nature of T cell-clonal expansions in response to AAV dosing and the relationship with TMA and other SAEs. These findings contribute to the ongoing efforts to optimize and improve gene therapy strategies for DMD and other genetically inherited diseases.

MATERIALS AND METHODS

Human subjects

The five subjects described in this manuscript participated in a phase 1b clinical trial designed to test the safety of systemically delivered AAV9-mini-dystrophin (PF-06939926 fordadistrogene movaparvovec) in DMD patients. The trial was sponsored by Pfizer. The study was conducted in compliance with ethical principles of the Declaration of Helsinki and all International Conference on Harmonisation Good Clinical Practice Guidelines. The protocol was approved by the relevant institutional review board/independent ethics committee at each study site. All participants (or parent/legal guardian) provided written informed consent.

PBMC culture, stimulation, and processing for 10x genomics

Blood was collected into sodium heparin tubes, and PBMCs were isolated using a Ficoll gradient, and cryopreserved in CTL-Cryo medium (Cellular Technology Limited, Cleveland, OH). PBMC vials pre- and post-AAV9 mini-dystrophin treatment were thawed in a 37°C water bath for 2–3 min. Thawed PBMCs were transferred to RPMI-C media consisting of RPMI 1640 (Gibco) supplemented with 10% fetal bovine serum (FBS, Thermo Fisher), 1% GlutaMAX (Thermo Fisher), 1% penicillin/streptomycin (P/S, Thermo Fisher), 1% non-essential amino acids (Thermo Fisher), and 1% 1M HEPES (Gibco). Cells were then centrifuged to remove cryopreservation media and resuspended in RPMI-C. Resuspended PBMCs were then seeded at 1.0×10^7 cells/mL/well in a 24-well plate format and stimulated with a pool of 146 peptides spanning the AAV serotype 9 capsid (Mimotopes) at 1.0 μg/mL overnight (16 h). Following overnight stimulation, PBMCs were harvested from the 24-well plate for immunomagnetic depletion of dead cells via Annexin V (StemCell Technologies) according to the manufacturer's instructions. Live PBMCs were centrifuged and resuspended in DPBS (Thermo Fisher) supplemented with 0.04% BSA (Millipore Sigma) as recommended by 10x Genomics for single-cell capture using Chromium (10x Genomics). Among the five participants, 111,300 PBMCs were sequenced from samples collected pre- and post-AAV9 mini-dystrophin dosing, with an average of 43,155 reads per cell (Table S2).

AAV9 peptides for PBMC exposure prior to single-cell sequencing

AAV9 peptides from Mimotopes were ordered to span the entire capsid gene encoding AAV serotype 9. Peptides contained an overlap of 10 amino acids and an offset of five amino acids were used to create a pool of 146 peptides.

AAV9 and mini-dystrophin IFN-γ ELISPOT

IFN-γ ELISpot was performed using the human IFN-γ ELISpot Plus kit (Mabtech) according to the manufacturer's instructions. In brief, the ELISpot plate was washed four times with DPBS (Thermo Fisher). The plate was then conditioned with 200 μL RPMI-C for 30 min at room temperature. PBMCs were then seeded at 4.0×10^5 cells/well incubated with 1 μg/mL of three different AAV9 or mini-dystrophin peptide pools, with a final volume of 250 μL/well for overnight stimulation (24 h). PBMCs were removed from the ELISpot plate and wells were rinsed five times with DPBS. After washing, the detection antibody was added (100 μL/well) and incubated for 1 h at room temperature. The detection antibody was removed, and the plate was washed an additional five times with DPBS, and ready-to-use TMB substrate solution (100 μL/well) was added for the plate to develop within 5 min. TMB development was stopped by washing the plate extensively with sterile ddH_2O (Thermo Fisher). After washing and drying, the spots were counted using an ELISpot plate reader (CTL ImmunoSpot). Results were reported as the mean spot count for three replicate wells.

10x library preparation, sequencing, alignment, and single-cell data analysis and clustering

Single-cell 5′ mRNA and TCR A/B libraries were generated using Chromium Single Cell 5′ v.2 (10x Genomics). scRNA and scTCR libraries were sequenced using NovaSeq 6000 S4 (Illumina) 2×100 base pairs (bp) paired-end reading strategy. The raw GEX and VDJ libraries were mapped to the human reference genome GRCH38 2020-A and to vdj_GRCh38_alts_ensembl-5.0.0 using cellranger count (version 6.1.2) from 10x Genomics. The filtered_feature_bc_matrix cellranger outputs were analyzed using the R package Seurat (version 4.0).[16] Cells with more than 20% mitochondrial expression and less than 200 or more than 5,200 unique features were removed. UMI counts were log normalized using NormalizeData default parameters, FindVariableFeatures to select the 2,000 highest variable genes and integrated using SelectIntegrationFeatures, FindIntegrationAnchors, and IntegrateData functions. We then used ScaleData, FindNeighbors, and RunUMAP, FindNeighbors, and FindClusters at 30 components for uniform manifold approximation and projection (UMAP) visualization. We used Azimuth[17] to automatically assign cell type annotations with the Human - PBMC dataset as reference.[50] Next, we followed by integrating the expansion data the Seurat dataset for downstream differential expression analysis of cells and visualization. For subcluster analysis, we used "predicted.celltype.l2" annotations. The scCustomize package was used to generate some visualizations.[51]

Gene set enrichment analysis

GSEA was performed with the WEB-based Gene Set Analysis Tool Kit (https://www.webgestalt.org/) using the gene ontology-biological process (GO-BP) database to identify enriched pathways using differentially expressed genes identified by comparing pre- and post-AAV administration time points.[52]

TCR clumping analysis

TCR clumping analysis was performed using the CoNGA package.[23] Briefly, TCR clumping analysis identifies neighborhoods of sequence convergence in TCR space at greater density than expected by chance under a simple null model of VDJ rearrangement. For each TCR in the dataset, we count how many TCRs are within a set of fixed TCRdist radii of 24, 48, 72, and 96 units, and compare that number to the expected number given the size of the dataset using the Poisson model. Shuffling the paired TCR chains and measuring the distances of these shuffled pairs is used to create the background and estimate its distance distributions. The Benjamini-Hochberg method for controlling the FDR is applied on a per-TCR basis across all radii tested.

ADA titers against AAV9 and mini-dystrophin

To measure antibodies against mini-dystrophin, samples were diluted in diluent buffer (Blocker Casein in PBS, Thermo Fisher) and incubated with biotin-labeled mini-dystrophin-FLAG and ruthenium-labeled mini-dystrophin-FLAG for 3h at RT. The samples were then added to streptavidin-coated MesoScaleDiscovery plates to capture complexes of antibodies bound to both the ruthenium and biotinylated mini-dys-FLAG, and tripropylamine was added to produce an electrochemiluminescent signal.

To measure antibodies directed against AAV9, 96-well ELISA plates were coated with 1e10 vg/mL AAV9-mini-dystrophin. After blocking, plates were incubated with samples diluted in PBS with 0.05% polysorbate-20 and 1% BSA. Plates were washed and incubated with biotinylated AAV9-mini-dystrophin for 1 h at RT. Plates were washed again and incubated with HRP-avidin D (Vector Labs) for 30 min at RT. After a final wash, reactions were developed with tetramethylbenzidine peroxidase, stopped with 0.18M sulfuric acid, and read at 450 nm on a plate reader (Bio-Tek PowerWave HT).

DATA AND CODE AVAILABILITY

Data generated during this study will be included in this published article. scRNA-seq sequences will be deposited in the NCBI Gene Expression Omnibus database. Processed data generated during this study are available on Zenodo (https://zenodo.org/records/13935259).

ACKNOWLEDGMENTS

The authors thank and acknowledge the use of services from the following cores: the UCLA Technology Center for Genomics & Bioinformatics (TCGB) and the UCLA Institute for Quantitative and Computational Biosciences (QC Bio). This study was supported by the Department of Defense (to M.J.S. and S.A.V.); NIH (NINDS-R01NS117912 to M.J.S.; NIAMS-R01NS120060 to S.A.V. and P50AR052646 (to E.M.M. and M.J.S.); R01HL061322 and R01NS047726 (to E.M.M.); NIAID R01AI136514, U01AI150747, and R21AI169085 (to P.G.T.); the Cystic Fibrosis Foundation (PTAC postdoc-faculty transition award to M.A.B.); and the American Lebanese Syrian Associated Charities (to P.G.T.).

AUTHOR CONTRIBUTIONS

Conceptualization: M.J.S., M.R.E., S.A.V., J.O., M.A.B., and L.O.W. Methodology: M.R.E., M.A.B., S.A.S., C.S.Y., S.C., T.A.L., S.A.V., and M.J.S. Visualization: M.R.E., M.J.S., and C.S.Y. Project Administration: M.J.S., M.R.E., and M.A.B. Investigation: M.R.E., M.A.B., T.A.L., C.S.Y., S.A.S., and A.E. Software, Data Curation: S.A.S. Formal analysis: M.R.E., A.E., S.A.S., M.A.B., and M.J.S. Writing – Original Draft: M.R.E., M.J.S., and M.A.B. Writing – Review and Editing: all authors. Resources: UCLA Technology Center for Genomics and Biotechnology, UCLA Health Jonsson Comprehensive Cancer Center, UCLA Broad Stem Cell Center Flow Core. Supervision: M.J.S., P.G.T., and S.A.S. Funding Acquisition: M.J.S., S.A.V., E.M.M., P.G.T., and M.A.B.

DECLARATION OF INTERESTS

M.J.S. and C.S.Y. are co-founders of MyoGene Bio, a startup spun out of UCLA developing gene editing therapies for DMD. C.S.Y. and M.R.E. are employees of MyoGene Bio. M.A.B. is a listed inventor on a pending patent relating to AAV gene therapy (WO 2021/242664 A1).

SUPPLEMENTAL INFORMATION

Supplemental information can be found online at https://doi.org/10.1016/j.omtm.2024.101349.

REFERENCES

1. Harper, S.Q., Hauser, M.A., DelloRusso, C., Duan, D., Crawford, R.W., Phelps, S.F., Harper, H.A., Robinson, A.S., Engelhardt, J.F., Brooks, S.V., and Chamberlain, J.S. (2002). Modular flexibility of dystrophin: implications for gene therapy of Duchenne muscular dystrophy. Nat. Med. *8*, 253–261. https://doi.org/10.1038/nm0302-253.

2. Manno, C.S., Pierce, G.F., Arruda, V.R., Glader, B., Ragni, M., Rasko, J.J., Ozelo, M.C., Hoots, K., Blatt, P., Konkle, B., et al. (2006). Successful transduction of liver in hemophilia by AAV-Factor IX and limitations imposed by the host immune response. Nat. Med. *12*, 342–347. https://doi.org/10.1038/nm1358.

3. Salabarria, S.M., Corti, M., Coleman, K.E., Wichman, M.B., Berthy, J.A., D'Souza, P., Tifft, C.J., Herzog, R.W., Elder, M.E., Shoemaker, L.R., et al. (2024). Thrombotic microangiopathy following systemic AAV administration is dependent on anti-capsid antibodies. J. Clin. Invest. *134*, e173510. https://doi.org/10.1172/JCI173510.

4. Shen, W., Liu, S., and Ou, L. (2022). Corrigendum: rAAV immunogenicity, toxicity, and durability in 255 clinical trials: A meta-analysis. Front. Immunol. *13*, 1104646. https://doi.org/10.3389/fimmu.2022.1104646.

5. Shen, W., Liu, S., and Ou, L. (2022). rAAV immunogenicity, toxicity, and durability in 255 clinical trials: A meta-analysis. Front. Immunol. *13*, 1001263. https://doi.org/10.3389/fimmu.2022.1001263.

6. Witte, D., Hartmann, H., Drube, J., Haffner, D., and Illsinger, S. (2022). [Thrombotic Microangiopathy (TMA) after Gene Replacemant Therapy (GRT) due to Spinal Muscular Atrophy: Case Summary and Recommendations for Treatment]. Klin. Pädiatr. *234*, 42–47. https://doi.org/10.1055/a-1538-4936.

7. Zaiss, A.K., Cotter, M.J., White, L.R., Clark, S.A., Wong, N.C.W., Holers, V.M., Bartlett, J.S., and Muruve, D.A. (2008). Complement is an essential component of the immune response to adeno-associated virus vectors. J. Virol. *82*, 2727–2740. https://doi.org/10.1128/JVI.01990-07.

8. Matsumoto, A.K., Kopicky-Burd, J., Carter, R.H., Tuveson, D.A., Tedder, T.F., and Fearon, D.T. (1991). Intersection of the complement and immune systems: a signal transduction complex of the B lymphocyte-containing complement receptor type 2 and CD19. J. Exp. Med. *173*, 55–64. https://doi.org/10.1084/jem.173.1.55.

9. Tuveson, D.A., Ahearn, J.M., Matsumoto, A.K., and Fearon, D.T. (1991). Molecular interactions of complement receptors on B lymphocytes: a CR1/CR2 complex distinct from the CR2/CD19 complex. J. Exp. Med. *173*, 1083–1089. https://doi.org/10.1084/jem.173.5.1083.

10. Molina, H., Holers, V.M., Li, B., Fung, Y., Mariathasan, S., Goellner, J., Strauss-Schoenberger, J., Karr, R.W., and Chaplin, D.D. (1996). Markedly impaired humoral immune response in mice deficient in complement receptors 1 and 2. Proc. Natl. Acad. Sci. USA *93*, 3357–3361. https://doi.org/10.1073/pnas.93.8.3357.

11. Ahearn, J.M., Fischer, M.B., Croix, D., Goerg, S., Ma, M., Xia, J., Zhou, X., Howard, R.G., Rothstein, T.L., and Carroll, M.C. (1996). Disruption of the Cr2 locus results in a reduction in B-1a cells and in an impaired B cell response to T-dependent antigen. Immunity *4*, 251–262. https://doi.org/10.1016/s1074-7613(00)80433-1.

12. Kopf, M., Abel, B., Gallimore, A., Carroll, M., and Bachmann, M.F. (2002). Complement component C3 promotes T-cell priming and lung migration to control acute influenza virus infection. Nat. Med. *8*, 373–378. https://doi.org/10.1038/nm0402-373.

13. Smith, C.J., Ross, N., Kamal, A., Kim, K.Y., Kropf, E., Deschatelets, P., Francois, C., Quinn, W.J., 3rd, Singh, I., Majowicz, A., et al. (2022). Pre-existing humoral immunity and complement pathway contribute to immunogenicity of adeno-associated virus (AAV) vector in human blood. Front. Immunol. *13*, 999021. https://doi.org/10.3389/fimmu.2022.999021.

14. Emami, M.R., Espinoza, A., Young, C.S., Ma, F., Farahat, P.K., Felgner, P.L., Chamberlain, J.S., Xu, X., Pyle, A.D., Pellegrini, M., et al. (2023). Innate and adaptive AAV-mediated immune responses in a mouse model of Duchenne muscular dystrophy. Mol. Ther. Methods Clin. Dev. *30*, 90–102. https://doi.org/10.1016/j.omtm.2023.06.002.

15. Bonnemann, C.G., Belluscio, B.A., Braun, S., Morris, C., Singh, T., and Muntoni, F. (2023). Dystrophin Immunity after Gene Therapy for Duchenne's Muscular Dystrophy. N. Engl. J. Med. *388*, 2294–2296. https://doi.org/10.1056/NEJMc2212912.

16. Butler, A., Hoffman, P., Smibert, P., Papalexi, E., and Satija, R. (2018). Integrating single-cell transcriptomic data across different conditions, technologies, and species. Nat. Biotechnol. *36*, 411–420. https://doi.org/10.1038/nbt.4096.

17. Hao, Y., Hao, S., Andersen-Nissen, E., Mauck, W.M., 3rd, Zheng, S., Butler, A., Lee, M.J., Wilk, A.J., Darby, C., Zager, M., et al. (2021). Integrated analysis of multimodal single-cell data. Cell *184*, 3573–3587.e29. https://doi.org/10.1016/j.cell.2021.04.048.

18. Yu, J., and Liu, S.L. (2019). Emerging Role of LY6E in Virus-Host Interactions. Viruses *11*, 1020. https://doi.org/10.3390/v11111020.

19. Upadhyay, G. (2019). Emerging Role of Lymphocyte Antigen-6 Family of Genes in Cancer and Immune Cells. Front. Immunol. *10*, 819. https://doi.org/10.3389/fimmu.2019.00819.

20. Grosso, J.F., Kelleher, C.C., Harris, T.J., Maris, C.H., Hipkiss, E.L., De Marzo, A., Anders, R., Netto, G., Getnet, D., Bruno, T.C., et al. (2007). LAG-3 regulates CD8+ T cell accumulation and effector function in murine self- and tumor-tolerance systems. J. Clin. Invest. *117*, 3383–3392. https://doi.org/10.1172/jci31184.

21. Slevin, S.M., Garner, L.C., Lahiff, C., Tan, M., Wang, L.M., Ferry, H., Greenaway, B., Lynch, K., Geremia, A., Hughes, S., et al. (2020). Lymphocyte Activation Gene (LAG)-3 Is Associated With Mucosal Inflammation and Disease Activity in Ulcerative Colitis. J. Crohns Colitis *14*, 1446–1461. https://doi.org/10.1093/ecco-jcc/jjaa054.

22. Burnell, S.E.A., Capitani, L., MacLachlan, B.J., Mason, G.H., Gallimore, A.M., and Godkin, A. (2022). Seven mysteries of LAG-3: a multi-faceted immune receptor of increasing complexity. Immunother. Adv. *2*, ltab025. https://doi.org/10.1093/immadv/ltab025.

23. Schattgen, S.A., Guion, K., Crawford, J.C., Souquette, A., Barrio, A.M., Stubbington, M.J.T., Thomas, P.G., and Bradley, P. (2022). Integrating T cell receptor sequences and transcriptional profiles by clonotype neighbor graph analysis (CoNGA). Nat. Biotechnol. *40*, 54–63. https://doi.org/10.1038/s41587-021-00989-2.

24. Dash, P., Fiore-Gartland, A.J., Hertz, T., Wang, G.C., Sharma, S., Souquette, A., Crawford, J.C., Clemens, E.B., Nguyen, T.H.O., Kedzierska, K., et al. (2017). Quantifiable predictive features define epitope-specific T cell receptor repertoires. Nature *547*, 89–93. https://doi.org/10.1038/nature22383.

25. Mayer-Blackwell, K., Schattgen, S., Cohen-Lavi, L., Crawford, J.C., Souquette, A., Gaevert, J.A., Hertz, T., Thomas, P.G., Bradley, P., and Fiore-Gartland, A. (2021). TCR meta-clonotypes for biomarker discovery with tcrdist3 enabled identification of public, HLA-restricted clusters of SARS-CoV-2 TCRs. Elife *10*, e68605. https://doi.org/10.7554/eLife.68605.

26. Mendell, J., Sahenk, Z., Lehman, K., Lowes, L., Reash, N., Iammarino, M., Alfano, L., Lewis, S., Church, K., Shell, R., et al. (2023). Long-term Safety and Efficacy in Patients with DMD 4 Years Post-Treatment with Delandistrogene Moxeparvovec (SRP-9001) in a Phase 1/2a Study (P3-8.006). Neurology *100*, 3700. https://doi.org/10.1212/wnl.0000000000203462.

27. Lek, A., Atas, E., Hesterlee, S.E., Byrne, B.J., and Bönnemann, C.G. (2023). Meeting Report: 2022 Muscular Dystrophy Association Summit on 'Safety and Challenges in Gene Transfer Therapy'. J. Neuromuscul. Dis. *10*, 327–336. https://doi.org/10.3233/JND-221639.

28. Sajid, M., Ullah, H., Yan, K., He, M., Feng, J., Shereen, M.A., Hao, R., Li, Q., Guo, D., Chen, Y., and Zhou, L. (2021). The Functional and Antiviral Activity of Interferon Alpha-Inducible IFI6 Against Hepatitis B Virus Replication and Gene Expression. Front. Immunol. *12*, 634937. https://doi.org/10.3389/fimmu.2021.634937.

29. DeDiego, M.L., Martinez-Sobrido, L., and Topham, D.J. (2019). Novel Functions of IFI44L as a Feedback Regulator of Host Antiviral Responses. J. Virol. *93*, e01159-19. https://doi.org/10.1128/jvi.01159-19.

30. Weiss, C.M., Trobaugh, D.W., Sun, C., Lucas, T.M., Diamond, M.S., Ryman, K.D., and Klimstra, W.B. (2018). The Interferon-Induced Exonuclease ISG20 Exerts Antiviral Activity through Upregulation of Type I Interferon Response Proteins. mSphere *3*, e00209-18. https://doi.org/10.1128/mSphere.00209-18.

31. Tolomeo, M., Cavalli, A., and Cascio, A. (2022). STAT1 and Its Crucial Role in the Control of Viral Infections. Int. J. Mol. Sci. *23*, 4095. https://doi.org/10.3390/ijms23084095.

32. Verhelst, J., Hulpiau, P., and Saelens, X. (2013). Mx proteins: antiviral gatekeepers that restrain the uninvited. Microbiol. Mol. Biol. Rev. *77*, 551–566. https://doi.org/10.1128/mmbr.00024-13.

33. Pagani, I., Poli, G., and Vicenzi, E. (2021). TRIM22. A Multitasking Antiviral Factor. Cells *10*, 1864. https://doi.org/10.3390/cells10081864.

34. Bercovici, N., Duffour, M.T., Agrawal, S., Salcedo, M., and Abastado, J.P. (2000). New methods for assessing T-cell responses. Clin. Diagn. Lab. Immunol. *7*, 859–864. https://doi.org/10.1128/cdli.7.6.859-864.2000.

35. Zimmerer, J.M., Lesinski, G.B., Ruppert, A.S., Radmacher, M.D., Noble, C., Kendra, K., Walker, M.J., and Carson, W.E., 3rd (2008). Gene expression profiling reveals similarities between the *in vitro* and *in vivo* responses of immune effector cells to IFN-alpha. Clin. Cancer Res. *14*, 5900–5906. https://doi.org/10.1158/1078-0432.Ccr-08-0846.

36. Meckiff, B.J., Ramírez-Suástegui, C., Fajardo, V., Chee, S.J., Kusnadi, A., Simon, H., Eschweiler, S., Grifoni, A., Pelosi, E., Weiskopf, D., et al. (2020). Imbalance of Regulatory and Cytotoxic SARS-CoV-2-Reactive CD4(+) T Cells in COVID-19. Cell *183*, 1340–1353.e16. https://doi.org/10.1016/j.cell.2020.10.001.

37. Fuchs, Y.F., Sharma, V., Eugster, A., Kraus, G., Morgenstern, R., Dahl, A., Reinhardt, S., Petzold, A., Lindner, A., Löbel, D., and Bonifacio, E. (2019). Gene Expression-Based Identification of Antigen-Responsive CD8(+) T Cells on a Single-Cell Level. Front. Immunol. *10*, 2568. https://doi.org/10.3389/fimmu.2019.02568.

38. Ivashkiv, L.B. (2018). IFNγ: signalling, epigenetics and roles in immunity, metabolism, disease and cancer immunotherapy. Nat. Rev. Immunol. *18*, 545–558. https://doi.org/10.1038/s41577-018-0029-z.

39. Cao, Q., Wu, S., Xiao, C., Chen, S., Chi, X., Cui, X., Tang, H., Su, W., Zheng, Y., Zhong, J., et al. (2021). Integrated single-cell analysis revealed immune dynamics during Ad5-nCoV immunization. Cell Discov. *7*, 64. https://doi.org/10.1038/s41421-021-00300-2.

40. Chattopadhyay, P., Khare, K., Kumar, M., Mishra, P., Anand, A., Maurya, R., Gupta, R., Sahni, S., Gupta, A., Wadhwa, S., et al. (2022). Single-cell multiomics revealed the dynamics of antigen presentation, immune response and T cell activation in the COVID-19 positive and recovered individuals. Front. Immunol. *13*, 1034159. https://doi.org/10.3389/fimmu.2022.1034159.

41. Lee, J.S., Park, S., Jeong, H.W., Ahn, J.Y., Choi, S.J., Lee, H., Choi, B., Nam, S.K., Sa, M., Kwon, J.S., et al. (2020). Immunophenotyping of COVID-19 and influenza highlights the role of type I interferons in development of severe COVID-19. Sci. Immunol. *5*, eabd1554. https://doi.org/10.1126/sciimmunol.abd1554.

42. Melms, J.C., Biermann, J., Huang, H., Wang, Y., Nair, A., Tagore, S., Katsyv, I., Rendeiro, A.F., Amin, A.D., Schapiro, D., et al. (2021). A molecular single-cell lung atlas of lethal COVID-19. Nature *595*, 114–119. https://doi.org/10.1038/s41586-021-03569-1.

43. Stephenson, E., Reynolds, G., Botting, R.A., Calero-Nieto, F.J., Morgan, M.D., Tuong, Z.K., Bach, K., Sungnak, W., Worlock, K.B., Yoshida, M., et al. (2021). Single-cell multi-omics analysis of the immune response in COVID-19. Nat. Med. *27*, 904–916. https://doi.org/10.1038/s41591-021-01329-2.

44. Wang, Y., Wang, X., Luu, L.D.W., Li, J., Cui, X., Yao, H., Chen, S., Fu, J., Wang, L., Wang, C., et al. (2022). Single-cell transcriptomic atlas reveals distinct immunological responses between COVID-19 vaccine and natural SARS-CoV-2 infection. J. Med. Virol. *94*, 5304–5324. https://doi.org/10.1002/jmv.28012.

45. Zhu, L., Yang, P., Zhao, Y., Zhuang, Z., Wang, Z., Song, R., Zhang, J., Liu, C., Gao, Q., Xu, Q., et al. (2020). Single-Cell Sequencing of Peripheral Mononuclear Cells Reveals Distinct Immune Response Landscapes of COVID-19 and Influenza Patients. Immunity *53*, 685–696.e3. https://doi.org/10.1016/j.immuni.2020.07.009.

46. Belford, A., Myles, O., Magill, A., Wang, J., Myhand, R.C., and Waselenko, J.K. (2004). Thrombotic microangiopathy (TMA) and stroke due to human herpesvirus-6 (HHV-6) reactivation in an adult receiving high-dose melphalan with autologous peripheral stem cell transplantation. Am. J. Hematol. *76*, 156–162. https://doi.org/10.1002/ajh.20068.

47. Matsuda, Y., Hara, J., Miyoshi, H., Osugi, Y., Fujisaki, H., Takai, K., Ohta, H., Tanaka-Taya, K., Yamanishi, K., and Okada, S. (1999). Thrombotic microangiopathy associated with reactivation of human herpesvirus-6 following high-dose chemotherapy with autologous bone marrow transplantation in young children. Bone Marrow Transplant. *24*, 919–923. https://doi.org/10.1038/sj.bmt.1702003.

48. Java, A., Edwards, A., Rossi, A., Pandey, R., Gaut, J., Delos Santos, R., Miller, B., Klein, C., and Brennan, D. (2015). Cytomegalovirus-induced thrombotic microangiopathy after renal transplant successfully treated with eculizumab: case report and review of the literature. Transpl. Int. *28*, 1121–1125. https://doi.org/10.1111/tri.12582.

49. Flanigan, K.M., Campbell, K., Viollet, L., Wang, W., Gomez, A.M., Walker, C.M., and Mendell, J.R. (2013). Anti-dystrophin T cell responses in Duchenne muscular dystrophy: prevalence and a glucocorticoid treatment effect. Hum. Gene Ther. *24*, 797–806. https://doi.org/10.1089/hum.2013.092.

50. Borcherding, N., Bormann, N.L., and Kraus, G. (2020). scRepertoire: An R-based toolkit for single-cell immune receptor analysis. F1000Res. *9*, 47. https://doi.org/10.12688/f1000research.22139.2.

51. Marsh, S.E., and Truter, I. (2021). Improving health-related quality of life instrument translation into South African languages. S. Afr. Fam. Pract. *63*, e1–e11. https://doi.org/10.4102/safp.v63i1.5361.

52. Wang, J., Vasaikar, S., Shi, Z., Greer, M., and Zhang, B. (2017). WebGestalt 2017: a more comprehensive, powerful, flexible and interactive gene set enrichment analysis toolkit. Nucleic Acids Res. *45*. W130-w137. https://doi.org/10.1093/nar/gkx356.